Axially and radially quantized spin waves in thick permalloy nanodots

X. Zhou,[1] D. Kumar,[1] I. S. Maksymov,[2] M. Kostylev,[2] and A. O. Adeyeye[1,*]

[1]*Information Storage Materials Laboratory, Department of Electrical and Computer Engineering, National University of Singapore, Singapore 117576, Singapore*

[2]*School of Physics, University of Western Australia, Crawley, Western Australia 6009, Australia*

(Received 25 March 2015; revised manuscript received 26 June 2015; published 3 August 2015)

We have investigated the spin wave modes in perpendicularly magnetized permalloy nanodots as a function of film thickness using field modulated perpendicular ferromagnetic resonance spectroscopy. We observed mode intensity inversion with an increase in dot thickness. In thicker dots, one ellusive antisymmetric spin wave mode was also detected due to the asymmetric nature of the excitation signal. In the case of the thickest nanodot, a circulating chiral mode near the dot surface was also observed. Our experimental results are in good qualitative agreement with the dynamic micromagnetic simulations.

DOI: 10.1103/PhysRevB.92.054401 PACS number(s): 62.23.Eg, 75.30.Ds, 75.40.Gb, 76.50.+g

I. INTRODUCTION

Spin waves [1,2], defined as coherent excitations of spin degree of freedom in a magnetic medium, are of significant interest and have received huge attention in the past decade. This is largely due to advances in controlled nanofabrication techniques, which allow the synthesis of high quality magnetic nanostructures with sizes much smaller than the typical spin wave free propagation path, and the development of advanced characterization techniques. Additional factors, such as extrinsic control of the spin wave band structure [3,4], low energy consumption devices [5,6], and the potential for a symbiotic coexistence with the current information processing (technological) ecosystem [7,8], continue to promote research in this field [9].

Spin waves span the microwave and the submillimeter wave frequency bands, and their wavelengths can vary from 1 nm to several microns, exhibiting a diverse range of interesting phenomena at different length scales. Effects which highlight the wave and particle nature of spin waves have now been demonstrated in several submicron systems [10]. In a bulk ferromagnet, spin waves have one dispersive mode [11]. In an infinite thin film, multiple modes result due to the quantized modulation of dynamic magnetization along the film's thickness [12]. The orientation of the film's surface relative to the external magnetic field is also important [13]. If the thickness is reduced below a limit, typically known as the exchange length in a ferromagnet, the magnetization can become uniform along the thickness and multiple bands can collapse into a single one [14]. Several other interesting spin wave related phenomena have been observed in spin wave waveguides [15], nanowires [16,17], one- and two-dimensional magnonic crystals [18], and other types of confined magnetic nanostructures [19].

An exotic magnetic vortex topology has been observed and studied for certain thickness (l) to diameter (D) (aspect) ratios ($\xi = l/D$) [20]. In the case of perpendicularly magnetized nanodots (and wires), unconventional spin wave dynamics has been reported for $\xi \leqslant 0.2$ [21] and $D = 500\,\text{nm}$, or $\xi \approx 20$ (nanowire). Using a combination of mechanical ferromagnetic resonance (MFMR) [22] and micromagnetic simulations, de Loubens *et al.* [21] have been able to infer the mode profiles of up to three standing spin wave modes (for $\xi = 0.2$).

In this paper, we study the effect of thickness on the spin wave modes in nanodots with ξ in the range from 0.08 to 0.37 using the highly sensitive field modulated perpendicular ferromagnetic resonance (PFMR) technique [23]. In doing so, we experimentally demonstrate the existence of axially symmetric and antisymmetric and chiral spin wave modes. These findings, which enhance our knowledge of spin wave modes, could prove helpful in the design of spin wave based signal processing devices [7].

II. EXPERIMENTAL AND SIMULATION METHODS

Periodic two-dimensional arrays of isolated $Ni_{80}Fe_{20}$ (permalloy) dots with a diameter (D) of 300 nm, pitch (p) of 620 nm, and thicknesses l in the range from 25 to 110 nm were fabricated on a silicon substrate over a large area ($4 \times 4\,\text{mm}^2$) using deep ultraviolet (DUV) lithography at a 248 nm exposure wavelength, followed by electron beam evaporation and an ultrasonic assisted liftoff process in OK73 resist thinner. Permalloy dots were deposited at a constant rate of 0.2 Å/s with a base pressure of 2×10^{-8} Torr. This fabrication technique is a magnonic adaption of the DUV lithography technique commonly used in the semiconductor industry. Details of the fabrication process have also been described elsewhere [24].

A representative scanning electron microscopy (SEM) micrograph image of the tilted (viewing angle 35°) 85 nm thick permalloy dot array is shown in Fig. 1(a). These SEM images show good edge definition and uniformity.

The hysteresis loops of the dot arrays were characterized using a vibrating sample magnetometer (VSM). Shown in Fig. 1(b) is a normalized hysteresis loop of 85 nm thick dot arrays with the external magnetic field applied perpendicularly to the film plane (defined as the z direction). This loop has zero remanence and a saturation field of around 6 kOe. The inset of Fig. 1(b) is the corresponding hysteresis loop measured with the in-plane magnetic field. This hysteresis loop has a double triangle shape, typical for circular dots with a vortex ground state.

*Corresponding author: eleaao@nus.edu.sg

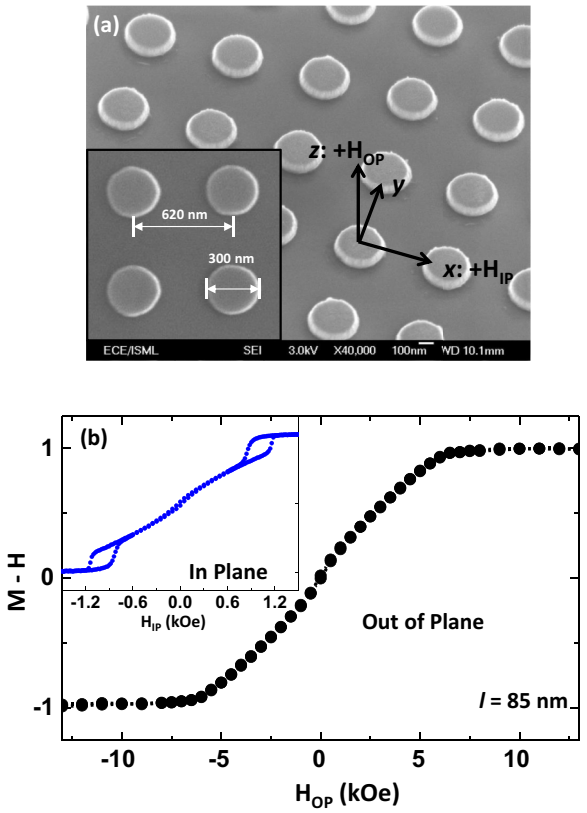

FIG. 1. (Color online) (a) SEM image (the viewing angle is 35°) of a permalloy circular dot array. The dot diameter is $d = 300$ nm, pitch $p = 620$ nm, and thickness $l = 85$ nm. (b) Hysteresis loop of a 85 nm thick dot array magnetized perpendicularly and in plane (inset) measured with VSM.

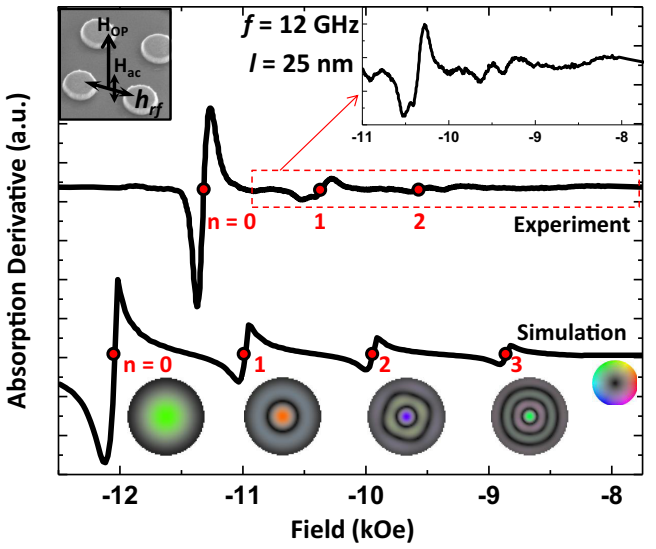

FIG. 2. (Color online) Comparison between the experimental PFMR spectra and simulated PFMR spectra for a 25 nm thick permalloy dot array at 12 GHz. The left inset is the sketch for the field geometry. The right inset is a zoom-in of the PFMR spectra in the field range from −11 to − 7.5 kOe. Shown below the simulated PFMR spectrum are the corresponding mode profiles for each of the four resonant modes ($n = 0,1,2$, and 3).

An interferometric phase detector was used to detect the PFMR signal with an ultralow signal-to-noise ratio. The high sensitivity of PFMR spectroscopy helped us detect several higher order modes, which would not be detectable using a conventional in-plane FMR measurement. In this setup, the 20 dBm microwave signal (h_{rf}) was generated by a continuous wave microwave generator at a specific frequency in the range from 9 to 14 GHz. The dot arrays were positioned on top of a 3 mils wide, 50 Ω microstrip board, with the dot arrays facing the board. A variable static magnetic field (H_{OP}) and an ac modulating field (H_{ac}) of ±20 Oe was applied along the z direction. A sketch of the field geometry is shown in the inset (top left) in Fig. 2. The output signal of the interferometric device is fed into a lock-in amplifier locked to the frequency of the ac modulating field. By fixing the excitation frequency and sweeping the bias field from −18 to − 6 kOe, the derivative of the microwave absorption spectra of the dot arrays was obtained. A high bias field was used to saturate the samples along the axis of the cylindrical nanodots (z direction) to ensure that experiments detect only spin wave modes and ignore any possible vortex gyration modes [25]. The bias field is applied coaxially so that it does not introduce any additional anisotropy in the system.

To validate the experimental results, simulation was performed on individual dots with a LLG MICROMAGNETICS [26] and object oriented micromagnetic framework (OOMMF) [27]. FMR spectra were obtained using LLG MICROMAGNETICS by calculating the real part of the dynamic susceptibility. In our LLG simulation, the ac excitation field was set at 10 Oe. Mode profiles were obtained by analyzing the data [14] produced from OOMMF. This is due to the differing capabilities of the two software packages. For the permalloy samples, we used a Landau-Lifshitz gyromagnetic ratio $|\gamma|$ of 2.21×10^5 m/As, damping constant α of 0.01, and a saturation magnetization M_s of 7.62×10^5 A/m was obtained experimentally from the 85 nm thick continuous film deposited at the same time as the patterned structures.

III. RESULTS AND DISCUSSION

Figure 2 shows the typical normalized experimental and simulated PFMR spectra of 25 nm thick dot arrays measured at 12 GHz. Multiple resonant modes were observed in the saturation region for both the experimental and simulation results, with the first mode exhibiting the highest intensity. Shown in the inset (top right) of Fig. 2 is a zoom-in of the FMR spectrum in the field magnitude range from 11 to 7.75 kOe. The intensity of the modes appears to monotonously decrease with the amplitude of the bias magnetic field. The experimental results are in qualitative agreement with the simulation results. The mode profiles obtained from OOMMF simulations are shown as insets in the figure. Here, the saturation and hue of the colors are determined by the intensity and phase of the mode, respectively. The modes $n = 0-3$ are labeled in the figure, where n corresponds to the number of radial nodes in the mode profile. The mode profile is uniform along the thickness of the nanodot and proportional to a zeroth-order Bessel function [28]. The lobes of each node are arranged in concentric annular rings with an alternating phase. The slight deformation

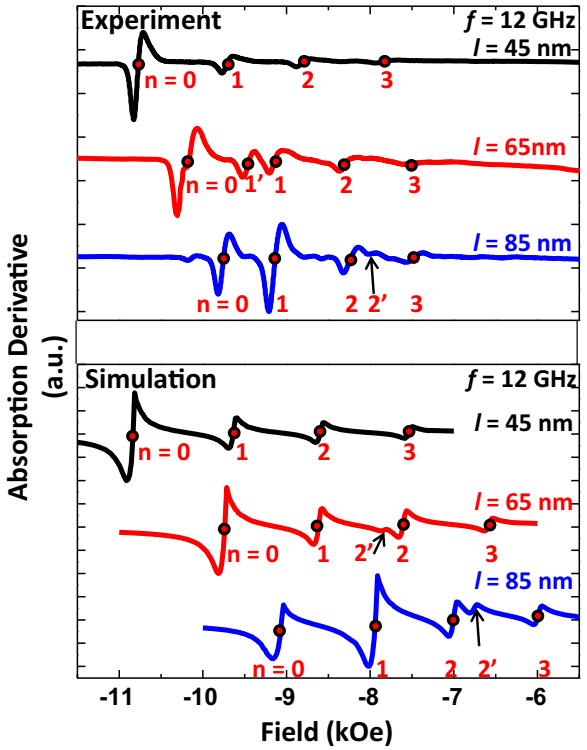

FIG. 3. (Color online) Comparison between the experimental PFMR spectra and simulated PFMR spectra for permalloy dot arrays with thicknesses of 45, 65, and 85 nm at 12 GHz.

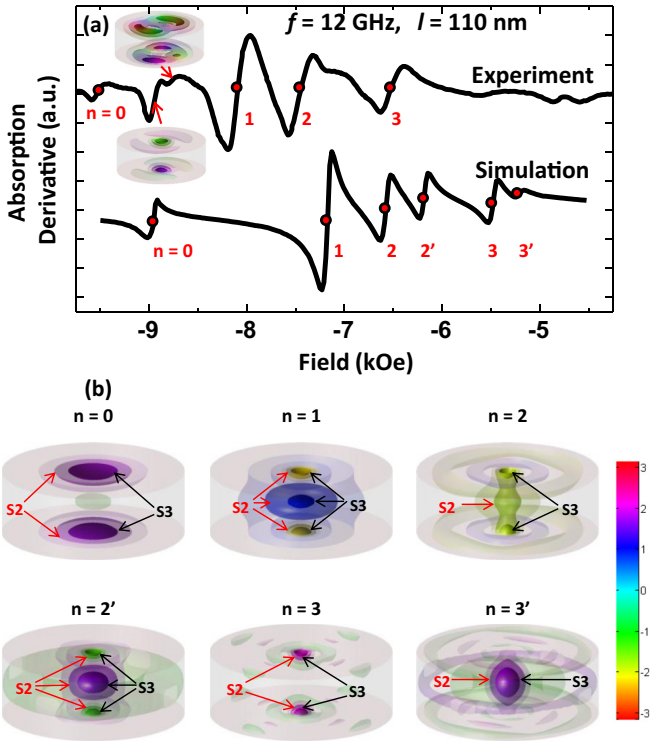

FIG. 4. (Color online) (a) Comparison between the experimental PFMR spectra and simulated PFMR spectra for a 110 nm thick permalloy dot array at 12 GHz. The insets show the mode profiles of the corresponding modes. (b) Mode profiles corresponding to the six resonant modes marked in (a). Surfaces S1 (not marked to avoid clutter), S2, and S3 denote the planes where the mode's amplitude is 25%, 50%, and 75% of its maximum value.

in the circular shape of some lobes may be attributed to the artificial anisotropy originating in the gridding, which occurs during most finite difference based simulations. Most of the power in these modes is dissipated in the central lobe.

To probe the effect of thickness on the PFMR spectra, nanodot arrays of thickness 45, 65, and 85 nm were also measured. A comparison of the experimental and simulated PFMR spectra taken at a frequency of 12 GHz is shown in Fig. 3. For convenience of comparison, all the spectra were normalized to the intensity of the strongest mode. Compared to 25 nm thick dot arrays, four modes are clearly visible in the PFMR spectrum of the 45 nm dot arrays due to a more pronounced signal. The field gap between neighboring modes is around 1 kOe. For dot arrays with a thickness of 65 nm, one more mode emerges at the field position near the second mode. During simulation, this additional mode appears close to the higher resonant field of the third mode. As the thickness of the dot arrays increases to 85 nm, the intensity of the second mode increases and becomes even larger than that of the first mode. Such an intensity inversion has also been reported in Refs. [21,29] in different samples. We also observed that with an increase in thickness, the resonant fields are shifting to lower bias fields due to the decreasing demagnetization field along the z direction. A slip between the experimental and simulated FMR spectra was observed. Two possible causes can be advanced to explain it. First, an inaccuracy is present regarding the values of the exchange constant A [30] and the gyrotropic ratio γ, which is not experimentally determined. Second, as the thickness increases, the presence of the dynamic dipolar coupling in between the single nanodots may affect the values of the resonant fields, although the qualitative form of the mode profile is not greatly altered, as can be seen from the figure given in the Supplemental Material [31]. This is verified by running the dynamic micromagnetic simulations with a two-dimensional periodical boundary condition (2D PBC). Henceforth, we wish to focus on the type of mode (qualitative) rather than its exact location on the field axis.

Figure 4(a) depicts the experimental and simulated PFMR spectra of the dot arrays with a thickness of 110 nm taken at a frequency of 12 GHz. Compared to the PFMR spectra taken for thinner dot arrays, the 110 nm thick dot arrays show a more complex PFMR spectrum due to mode quantization along the thickness. When compared to the case of $l = 85$ nm, the relative gain in the intensity of higher order modes appears to have increased with thickness. As seen in the simulated PFMR spectrum, a total of six modes can be observed in the saturation region. The mode profiles corresponding to these modes are numbered $n = 0$ to $n = 3'$ and are shown in Fig. 4(b). Here, the surfaces of successively reducing transparencies represent increasing mode amplitudes. The color of these surfaces denotes the phase of the mode profile. One nodal plane is expected between surfaces of any two different colors, indicating an out-of-phase oscillation. We interpret these modes based on the number of nodal points n_r encountered while moving radially outwards at the top (or bottom) end of the nanodot and the number of nodal points n_l seen while moving along the axis of the nanodot

cylinder. Thus, from Fig. 4(b), the set $\{n\} = \{0,1,2,2',3,3'\}$ can be mapped to a set of ordered pairs $\{(n_r,n_l)\} = \{(0,2), (1,2), (2,0), (2,2), (3,2), (3,0)\}$. From this we can see that mode $n = 0$ is a backward-volume-like mode, and $n = 2$ and $3'$ are as surface spin wave modes. Other modes are quantized in both radial and axial directions. We also note that n_r takes odd values while n_l does not. Odd values of n_r and n_l correspond to antisymmetric modes in the radial and axial directions, respectively.

In Fig. 4(a), we note that experimental and simulated results appear to agree qualitatively in terms of their relative field position, except one additional peak, which appears in the experimental observation. We suspect that this mode is an axially antisymmetric mode. For thinner dots the excitation field is uniform along the thickness, resulting in spin wave modes, which are symmetric and uniform along the film thickness. However, while experimenting with thicker samples, the excitation field can no longer qualify to be uniform along the thickness [32] and a slight antisymmetric component must be introduced. To understand the mode profile associated with this experimentally observed mode, we ran another simulation by applying the excitation signal in only one (x,z) quadrant of the nanodot. The mode profile thus obtained is shown besides the experimentally observed peak (lower inset). We now see $(n_r,n_l) = (1,1)$ for this mode. Here the top and bottom faces of the cylinder oscillate with a phase differing by π rad. Thus the set of experimentally observed modes for thickness $l = 110$ nm is $\{(0,2), (1,1), (1,2), (2,0), (3,2)\}$. The modes $\{(2,2), (3,0)\}$ are not well resolved in the PFMR spectrum.

The mode (1,2) has the most amplitude both in the experimental and simulated results. Such an intensity inversion for the vortex gyration mode has been discussed in Ref. [33] in some detail. We believe it is due to this reason that mode (0,1) is not noticeable in the results shown in Fig. 4(a). It is expected to occur at a higher field value than mode $n = 0$ (0,2), but it is also expected to have a much lower amplitude. All mode profiles presented in Fig. 4 share a rotational axis of symmetry with the axis of the cylindrical nanodot itself. This leads us to believe that the dot geometry and the associated shape anisotropy play a part in determining the spatial profile for a given mode. We also note that modes with a higher number of nodal lines are placed higher up in the frequency domain. This is also the case with modes on guitar strings or a drum membrane. We also note that a quantization in the radial direction increases the frequency more rapidly than a quantization in the axial direction—see the mode profiles for the (0,2) and (2,0) cases in Fig. 4(b). Similar observations have been discussed in Ref. [21] in the case of thinner (lower aspect ratio) dots as well.

To understand why the antisymmetric mode (1,1) is excited in our experiment, one more numerical simulation was run. It was shown previously that eddy currents may be responsible for the excitation of antisymmetric thickness modes in the nanostructures [34]. However, our simulation of microwave eddy currents for the present geometry demonstrated that, for a sparse array of circular nanodots with our sizes, the microwave eddy currents are strongly suppressed due to an essential discontinuity of the disk planar nanopattern.

Apart from the quantized spin wave modes, we also note the presence of a chiral mode in the experimentally obtained results. Simulation confirms that the mode is localized in a pair of annular rings at the top and bottom ends of the nanodot [cf. the upper inset next to the mode in Fig. 4(a)]. However, as opposed to the annular rings observed in Fig. 2, here the phase changes by 4π (shown by the change in hue), when we travel along the annuli. This represents a traveling spin wave mode (as opposed to the standing spin wave modes observed earlier) which circles around the ends of the nanodot. The chirality of this circling spin wave mode is the same (clockwise) at both the top and the bottom ends; however, they appear to be out of phase by about π rad.

IV. CONCLUSION

In conclusion, multiple quantized spin wave modes are observed for the dot arrays in the gigahertz frequency regime. As the thickness of the dot array increases, more spin wave modes, with quantization along the axial and radial directions, are detected. In addition, axially antisymmetric standing spin wave modes have been observed for thicker dots. We suppose that their excitation is enabled by some asymmetry of the excitation signal in the direction along the dot thickness. However, as the signal was symmetric in the azimuthal direction, no azimuthally quantized spin wave modes were detected. We also observed that with increasing thickness, an intensity inversion occurs where the modes with higher intensity have more nodal planes as well. Our experimental results were qualitatively validated using micromagnetic simulations.

ACKNOWLEDGMENT

This work was supported by the National Research Foundation, Prime Minister's Office, Singapore under its Competitive Research Programme (CRP Award No. NRF-CRP 10-2012-03), SMF-NUS New Horizon Awards, and Ministry of Education, Singapore AcRF Tier 2 (Grant No. R-263-000-A19-112).

[1] D. Stancil and A. Prabhakar, *Spin Waves: Theory and Applications* (Springer, Berlin, 2009).

[2] F. J. Dyson, Phys. Rev. **102**, 1217 (1956).

[3] A. V. Chumak, V. S. Tiberkevich, A. D. Karenowska, A. A. Serga, J. F. Gregg, A. N. Slavin, and B. Hillebrands, Nat. Commun. **1**, 141 (2010).

[4] J. W. Klos, D. Kumar, M. Krawczyk, and A. Barman, Sci. Rep. **3**, 2444 (2013).

[5] Z. Zeng, G. Finocchio, B. Zhang, P. K. Amiri, J. A. Katine, I. N. Krivorotov, Y. Huai, J. Langer, B. Azzerboni, K. L. Wang, and H. Jiang, Sci. Rep. **3**, 1426 (2013).

[6] H. Yu, G. Duerr, R. Huber, M. Bahr, T. Schwarze, F. Brandl, and D. Grundler, Nat. Commun. **4**, 2702 (2013).
[7] M. Krawczyk and D. Grundler, J. Phys.: Condens. Matter **26**, 123202 (2014).
[8] A. V. Chumak, A. A. Serga, and B. Hillebrands, Nat. Commun. **5**, 4700 (2014).
[9] L. S. Robert *et al.*, J. Phys. D: Appl. Phys. **47**, 333001 (2014).
[10] V. V. Kruglyak, S. O. Demokritov, and D. Grundler, J. Phys. D: Appl. Phys. **43**, 264001 (2010).
[11] C. Herring and C. Kittel, Phys. Rev. **81**, 869 (1951).
[12] S. K. Kim, J. Phys. D: Appl. Phys. **43**, 264004 (2010).
[13] B. A. Kalinikos and A. N. Slavin, J. Phys. C: Solid State Phys. **19**, 7013 (1986).
[14] D. Kumar, O. Dmytriiev, S. Ponraj, and A. Barman, J. Phys. D: Appl. Phys. **45**, 015001 (2012).
[15] J. W. Kłos, D. Kumar, M. Krawczyk, and A. Barman, Phys. Rev. B **89**, 014406 (2014).
[16] C. Mathieu *et al.*, Phys. Rev. Lett. **81**, 3968 (1998).
[17] Z. K. Wang, M. H. Kuok, S. C. Ng, D. J. Lockwood, M. G. Cottam, K. Nielsch, R. B. Wehrspohn, and U. Gösele, Phys. Rev. Lett. **89**, 027201 (2002).
[18] S. A. Nikitov, P. Tailhades, and C. S. Tsai, J. Magn. Magn. Mater. **236**, 320 (2001).
[19] B. Hillebrands and K. Ounadjela, *Spin Dynamics in Confined Magnetic Structures I* (Springer, Berlin, 2002).
[20] J. Ding, G. N. Kakazei, X. Liu, K. Y. Guslienko, and A. O. Adeyeye, Sci. Rep. **4**, 4796 (2014).
[21] G. de Loubens, V. V. Naletov, O. Klein, J. B. Youssef, F. Boust, and N. Vukadinovic, Phys. Rev. Lett. **98**, 127601 (2007).
[22] D. Rugar, C. S. Yannoni, and J. A. Sidles, Nature (London) **360**, 563 (1992).
[23] E. N. Ivanov and M. Kostylev, arXiv:1402.3459.
[24] A. O. Adeyeye and N. Singh, J. Phys. D: Appl. Phys. **41**, 153001 (2008).
[25] K. Y. Guslienko, X. F. Han, D. J. Keavney, R. Divan, and S. D. Bader, Phys. Rev. Lett. **96**, 067205 (2006).
[26] M. R. Scheinfein, LLG Micromagnetics Simulator, software for micromagnetic simulations, http://llgmicro.home.mindspring.com
[27] M. J. Donahue and D. G. Porter, The Object Oriented MicroMagnetic Framework (OOMMF) project at ITL/NIST, http://math.nist.gov/oommf
[28] G. N. Kakazei, P. E. Wigen, K. Y. Guslienko, V. Novosad, A. N. Slavin, V. O. Golub, N. A. Lesnik, and Y. Otani, Appl. Phys. Lett. **85**, 443 (2004).
[29] O. Klein, G. de Loubens, V. V. Naletov, F. Boust, T. Guillet, H. Hurdequint, A. Leksikov, A. N. Slavin, V. S. Tiberkevich, and N. Vukadinovic, Phys. Rev. B **78**, 144410 (2008).
[30] V. Castel, J. Ben Youssef, F. Boust, R. Weil, B. Pigeau, G. de Loubens, V. V. Naletov, O. Klein, and N. Vukadinovic, Phys. Rev. B **85**, 184419 (2012).
[31] See Supplemental Material at http://link.aps.org/supplemental/10.1103/PhysRevB.92.054401 for details of the comparison between simulation results on the single nanodot and nanodot arrays.
[32] Y.-Y. Au and S. Ingvarsson, J. Appl. Phys. **106**, 083906 (2009).
[33] J. Ding, G. N. Kakazei, X. M. Liu, K. Y. Guslienko, and A. O. Adeyeye, Appl. Phys. Lett. **104**, 192405 (2014).
[34] R. Bali, M. Kostylev, D. Tripathy, A. O. Adeyeye, and S. Samarin, Phys. Rev. B **85**, 104414 (2012).